YMTHE, Volume *28*

Supplemental Information

Spatiotemporal PET Imaging Reveals Differences in CAR-T Tumor Retention in Triple-Negative Breast Cancer Models

Alessia Volpe, Cameron Lang, Lindsay Lim, Francis Man, Ewelina Kurtys, Candice Ashmore-Harris, Preeth Johnson, Elena Skourti, Rafael T.M. de Rosales, and Gilbert O. Fruhwirth

SUPPLEMENTARY INFORMATION

This supplement contains Supplementary Methods detailing the generation of constructs, information about all used adherent cell lines, and methodologies describing lentivirus production, flow cytometric analyses, confocal fluorescence microscopy of T-cells and immunblotting. Moreover, it contains a Supplementary Table listing the used PCR primers for construct generation and several Supplementary Figures, which are referred to in the main text.

Supplementary Methods

Adherent Cells. HEK293T cells (ATCC) were grown in DMEM supplemented with 10% (v/v) heat-inactivated fetal calf serum (FCS), 100 IU/mL penicillin/streptomycin (P/S), and 2 mM *L*glutamine, and were used for lentivirus production. The following breast cancer cell lines (BCC) were used: MDA-MB-231 and MDA-MB-436 (both triple-negative BCC), HCC1954 (HER2 overexpressing BCC); MCF-7 (ER-positive BCC). MDA-MB-231.GFP-CaaX cells were generated as previously described[1] followed by fluorescence-activated cell sorting (FACS) to purify the population. All BCC cell lines were purchased from ATCC and maintained according to the supplier's recommendations. All cells were confirmed to free of mycoplasm throughout the study as determined by a PCR-based kit (Lookout kit, Sigma).

Cloning of expression cassettes CAR-T constructs. The constructs depicted in Fig.1A were generated in a lentiviral backbone to produce high-titre lentiviruses suitable for transduction of human T cells. Therefore, we synthesized a stretch of DNA starting on its 5' end with the recognition site of the restriction endonuclease *NotI* that is located within the T1E28z CAR, and encoding for the rest of this CAR.[2] This DNA piece was directly joined to a *SacII* restriction site and followed by the sequence encoding for the linker GTTRGGGAT and monomeric green fluorescent protein (EGFP A206K;[3]), another *SacII* restriction site, the sequence for the *Thosea asigna* (T2A) self-cleavage peptide, the sequence for the human NIS-monomeric TagRFP fusion reporter (NIS-RFP;[4]), and an *EcoRI* restriction site. This synthesized DNA piece (Genewizz) was sub-cloned into pcDNA3.1(-) MycHis-C (Life Technologies) between the *NotI* and *EcoRI* restriction endonuclease sites forming an intermediate construct (IC). The DNA encoding for 4αβ followed by a furin cleavage site, the T2A self-cleavage peptide and the T1E28z CAR was amplified by PCR with flanking *XhoI*/Kozak (5') and *KpnI* (3') sites using the corresponding SFG vector reported[5] as a template (for primers see Tab.S1). The resultant PCR product was gel purified, cut with *XhoI* and *NotI*, and sub-cloned into IC. IC was

then cut with *SacII* and re-ligated to remove the EGFP fused to the CAR, giving rise to a "Master" construct from which the various lentiviral constructs were generated: T4NT and T4 by cutting the corresponding constructs out with *XhoI* and *KpnI*, and sub-cloning them into the lentiviral vector backbone pLNT/SFFV[6]; for the control CAR T4ΔNT the relevant DNA piece was amplified from the Master construct by PCR (for primers see Tab.S1), cut with *XhoI* and *SacII*, and subcloned into the Master construct that was pre-cut with *XhoI* and *SacII*. The final lentiviral control construct was generated from this template by sub-cloning it into pLNT/SFFV using *XhoI* and *KpnI*.

Lentivirus production. Lentivirus production was performed using HEK293T cells as previously described.[6] Briefly, the packaging plasmids pΔ8.91 and pVSVG together with one of the lentiviral CAR/reporter plasmids (Fig.1A) were transfected into HEK293T cells. 20h after transfection, growth medium was replaced and virus-containing culture supernatants were harvested 36-48h later, concentrated four-fold using PEG-IT (SBI) and either used directly or stored at -80°C until use.

Flow cytometric analysis of T-cell markers. Phenotypes of transduced or untransduced T-cells were assessed by flow cytometry. Cells were fixed with 4% (w/v) paraformaldehyde (PFA) in phosphate buffered saline (PBS; pH 7.4) for 8 min at RT, twice PBS-washed, blocked (PBS containing 2% (w/v) bovine serum albumin (BSA) and 2% (v/v) FCS) for 15 min at RT, and stained for 60 min in PBS supplemented with 1% (v/v) FCS, 5 mM EDTA and the indicated antibodies. Used antibodies were specific for CD3 (clone OKT3, 2.5 µg/mL; BioLegend #317307), CD4 (clone SK3, 10 µg/mL, conjugated to FITC from BioLegend #344604), and CD8 (clone HIT8a, 0.6 µg/mL, conjugated to either PE or FITC from BioLegend #300907). For the analysis of CAR surface expression, we used an anti-human EGF monoclonal antibody (clone 10825, 1 µg/mL; R&D Systems #MAB236) followed by staining with phycoethrin-conjugated goat anti-mouse IgG (1 µg/mL, Dako). Data were acquired using a LSRFortessa II (BD Bioscience, UK) equipped with FACSDiva analysis software.

Flow cytometric analysis of checkpoint and B7-class inhibitory molecules on BCC. $4x10^5$ BCC were washed twice in PBS (pH 7.4) prior to cell resuspension in FACS buffer [PBS pH 7.4 containing 5 mM EDTA and 3% (v/v) FCS]. Antibody staining was done in two groups, with respective FMO controls ('fluorescence minus one' controls). Group 1: HLA-DR-APC

(clone L243, IgG2a, 1:50; Biolegend #307609), B7-H3-PE-Cy7 (clone MIH42, IgG1, 1:50; Biolegend #351007), B7-H4-PE (clone MIH43, IgG1, 1:50; Biolegend #358103), VISTA-FITC (clone B7H5DS8, IgG1, 1:50; ThermoFisher #11-1088-41), CD155-APC-Fire750 (clone SKII.4, IgG1, 1:50; Biolegend #337625). Group 2: Galectin-9-FITC (clone 9M1-3, IgG1, 1:50; Biolegend #348911), CAECAM-1-PE (clone CC1, IgG1, 1:50; ThermoFisher #12-0661-80), CD112-PE-Cy7 (clone TX31, IgG1, 1:50; Biolegend #337413). For all antibodies, cells were stained for 15 minutes at room temperature in the dark in FACS buffer [PBS pH 7.4, 5 mM EDTA, 3% FCS]. PD-L1 was analysed separately with a PE-conjugated anti-PD-L1 antibody (monoclonal rabbit; [28-8]; Abcam; 1 µg/mL, Dako). Data were acquired using either a BD FACS Melody (BD Bioscience, UK) or a LSRFortessa II (BD Bioscience, UK) instrument followed by analysis using FlowJo v10.6.2.

Confocal fluorescence microscopy of T-cells. Untransduced T-cells or CAR T-cells were plated onto retronectin-coated sterile glass cover slips (Ø13mm) placed into 24well plates. Cells were attached overnight under normal culture conditions and then stained alive with 2 µg/mL wheat germ agglutinin (WGA) conjugated to Alexa488 (plasma membrane stain in non-permeabilised cells) in growth medium for 30 min at 37°C in the dark. Cells were then fixed -with 4% (w/v) PFA in PBS for 8 min at RT, washed with PBS, and blocked (PBS containing 1% (w/v) BSA and 1% (v/v) goat serum). Cells were then incubated with the primary antibody mouse anti-EGFR (clone F4, CR-UK; 1 µg/mL in blocking solution; overnight at 4°C), thrice PBS-washed, and stained with Alexa647-conjugated goat anti-Mouse (Jackson Immunoresearch; 1 µg/mL in blocking solution; 45 min at RT) and Hoechst 33342 (1 µg/mL in PBS; 15 min at RT). Cells were washed twice with PBS and deionized water each before being mounted onto microscope slides using Mowiol-488 containing 2.5% (w/v) DABCO. All solutions were sterile filtered before use. Samples were dried overnight in the dark and imaged using a Nikon A1R confocal fluorescence microscope equipped with a 63x HCX PL APO CS uv NA1.3 WD0.28objective, lasers appropriate for imaging Hoechst 33342 (ex 405nm), Alexa488 (ex 488nm) and TagRFP (ex 561nm), and a spectral detector.

Immunoblotting. Cells were lysed in 1.2-fold lithium dodecyl sulphate (LDS)-based sample buffer (92.5 mM Tris/HCl pH 8.5, 0.75% (w/w) LDS, 3.75% (w/w) glycerol, 0.5 mM EDTA, 0.2 mM sodium orthovanadate, 10 nM calyculin A, 50 mM NaF, 1040 µM AEBSF, 800 nM aprotinin, 40 µM bestain, 14 µM E64 protease inhibitor, 20 µM leupeptin and 15 µM pepstatin

A) and lysates heated at 95°C for 20 min. Lysate protein concentrations were determined using the BCA protein assay (Thermo Fisher). Equal amounts of protein were supplemented with 100 mM DTT and 60 µM Serva Blue G250 (Serva), heated to 95°C for 5 min, and proteins separated by SDS-PAGE before being transferred to PVDF Immobilon-P membranes (EMD Millipore). Membranes were blocked with 4% (w/v) BSA in Tris-buffered saline containing 0.2% (w/v) Tween-20 (TBS-T) for 30 min, incubated with indicated primary antibody overnight at 4°C, washed four times with TBS-T, and incubated with a corresponding secondary antibody conjugated to horseradish peroxidase 60 min at room temperature. Signals were detected using an enhanced chemiluminescence detection system (ECL, Pierce) according to manufacturer's instructions together with a film processor.

Supplementary Table

Tab.S1. Primers used for the generation of the various CAR-T constructs.

Construct	Primer	Sequence
Master	Forward	5′-ACTTAGACTCGAGACCGCCATGGAGGCCGTGGAGACC-3′
	Reverse	5′-AAGGGTACCATATGTTACCGCGGGGGCAGGGCCTGC-3′
Master with truncated CAR	Forward	5′-ACTTAGACTCGAGACCGCCATGGAGGCCGTGGAGACC-3′
	Reverse	5′-CCGCGGCCGCGGCTTACTCCTCACCCAGAAAATAATAAAGG-3′

Supplementary References

1. Bear, JE, Loureiro, JJ, Libova, I, Fassler, R, Wehland, J, and Gertler, FB. **Negative regulation of fibroblast motility by Ena/VASP proteins**. *Cell*. 2000; **101**: 717-728.
2. Davies, DM, Foster, J, Van Der Stegen, SJ, Parente-Pereira, AC, Chiapero-Stanke, L, Delinassios, GJ, *et al.* **Flexible targeting of ErbB dimers that drive tumorigenesis by using genetically engineered T cells**. *Mol Med*. 2012; **18**: 565-576.
3. Zacharias, DA, Violin, JD, Newton, AC, and Tsien, RY. **Partitioning of lipid-modified monomeric GFPs into membrane microdomains of live cells**. *Science*. 2002; **296**: 913-916.
4. Fruhwirth, GO, Diocou, S, Blower, PJ, Ng, T, and Mullen, GE. **A whole-body dual-modality radionuclide optical strategy for preclinical imaging of metastasis and heterogeneous treatment response in different microenvironments**. *J Nucl Med*. 2014; **55**: 686-694.
5. Wilkie, S, Burbridge, SE, Chiapero-Stanke, L, Pereira, AC, Cleary, S, van der Stegen, SJ, *et al.* **Selective expansion of chimeric antigen receptor-targeted T-cells with potent effector function using interleukin-4**. *J Biol Chem*. 2010; **285**: 25538-25544.
6. Volpe, A, Man, F, Lim, L, Khoshnevisan, A, Blower, J, Blower, PJ, *et al.* **Radionuclide-fluorescence Reporter Gene Imaging to Track Tumor Progression in Rodent Tumor Models**. *J Vis Exp*. 2018; **133**: e57088.

Supplementary Figures

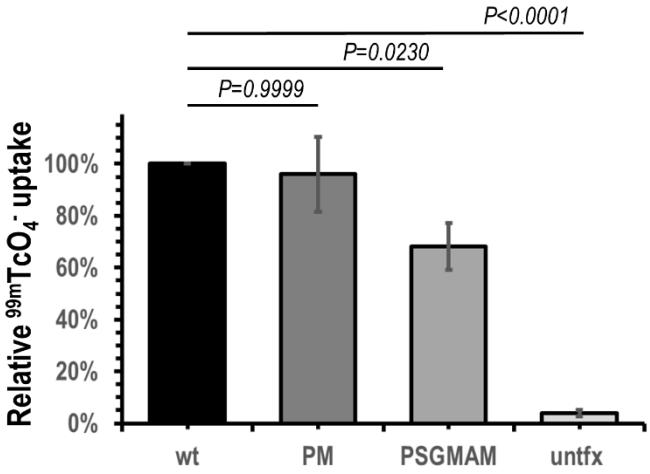

Supplementary Figure S1. Effect of N-terminal protein modifications on human iodide symporter (NIS) function | N-terminal protein sequence modifications of membrane proteins could result in intracellular mis-localization or altered protein turnover rates both affecting plasma membrane concentration, or direct effects on protein function. For NIS, the relevant read-out is overall reporter function, which is the combination of its concentration at the plasma membrane and actual substrate transport properties. This can be quantified on a cellular level by radiotracer $^{99m}TcO_4^-$ uptake. Due to the position in our construct platform (Fig.1A), the N-terminus of the NIS reporter would be modified with the minimal possible modification being the addition of an N-terminal proline (left-over from T2A self-cleavage), which would further cause the normally leading methionine not to be trimmed during processing resulting in PM being the minimal addition. Platform handling could have benefitted from a restriction endonuclease site between T2A and NIS providing more flexibility for potential reporter exchange. Consequently, we were interested in whether PM or relevant longer N-terminal NIS modifications (*i.e.* encoded by compatible restriction sites) would be functionally tolerated. Therefore, we generated NIS variants with the indicated N-terminal modifications and compared them to wildtype NIS. All variants were subcloned into the mammalian expression plasmid pcDNA3.1(+) and transfected into HEK293T cells for subsequent analysis of reporter function by $^{99m}TcO_4^-$ uptake. Uptake results were normalised to transfection efficiency. We found NIS to be sensitive to N-terminal modifications, but importantly, the shortest possible modification PM did not affect $^{99m}TcO_4^-$ transport rendering our strategy viable. Longer N-terminal modifications impeded NIS function (P<0.0001 for untransduced cells not expressing any NIS). Shown is transduction-normalised radiotracer uptake compared to wildtype NIS; error bars are SEM, cumulative data from N=3 biological repeats.

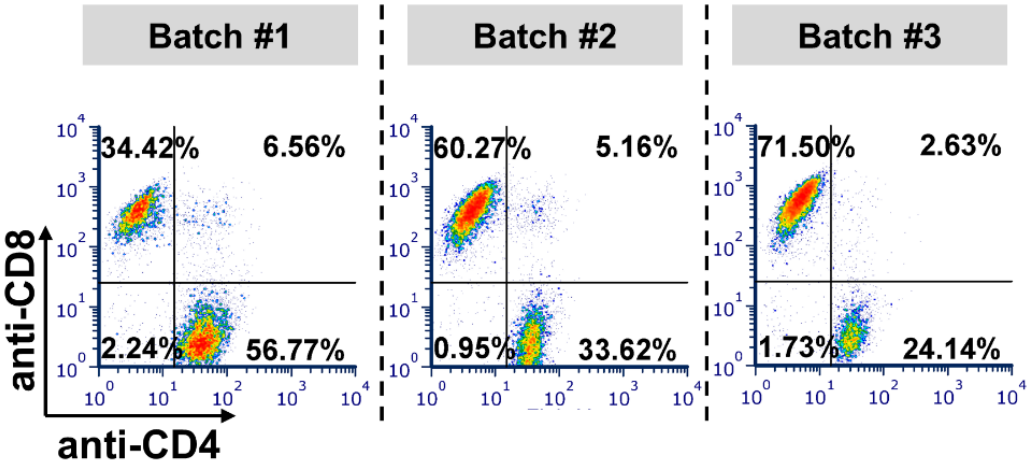

Supplementary Figure S2. CD4:CD8 ratios of T-cells from different donors used for CAR-T production | Three different blood batches (pooled from two to four donors each and anonymised) obtained from the National Blood Service were used for human T-cell isolation. Resultant human T-cells were analysed for relative CD4:CD8 ratios characterizing experimental input populations (after gating for CD3-positive cells).

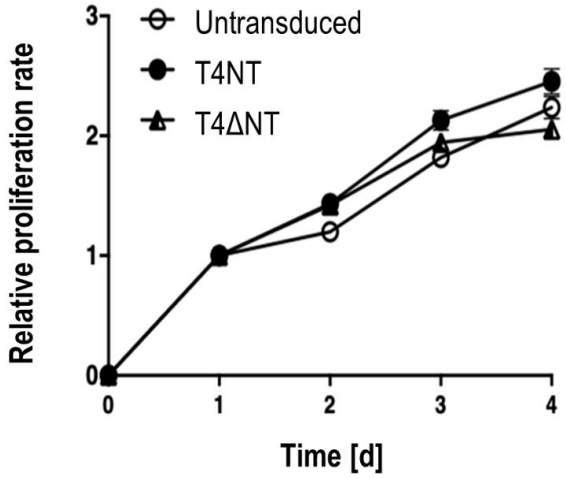

Supplementary Figure S3. Proliferation of T-cells and CAR T-cells | Proliferation data of untransduced T-cells in the presence of IL-2 compared to CAR T-cell proliferation in the presence of IL-4 (*cf.* selective expansion construct 4αβ in Fig.1). Data from the same isolated T-cell batch are shown and represent a typical CAR-T production compared to the parental T-cells. Each data point represents the mean ± SD from three parallel experiments from the same original isolated T-cell batch (*cf.* Supplementary Fig.S2). No significant proliferation differences were observed.

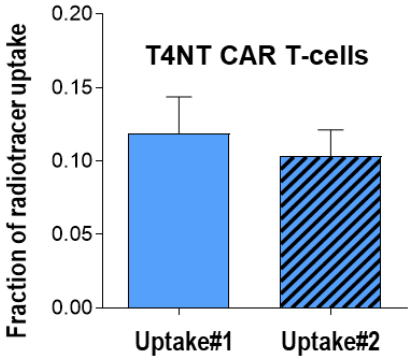

Supplementary Figure S4. Repeat radiotracer uptake in T4NT Car T-cells | T4NT CAR T-cells were subjected to a first $^{99m}TcO_4^-$ uptake assay, then resuspended in growth medium and incubated for 48h (after eight ^{99m}Tc half-lives 4‰ of the initial radioactivity was left) before a second uptake assay was performed under the same conditions as the first one. Shown is the radiotracer uptake (as a fraction of a NIS overexpressing reference cell line for experimental normalisation) for the same number of T4NT CAR T-cells. No significant differences were observed between repeat uptake assays (*N*=4; error bars are SEM; *P*=0.8958).

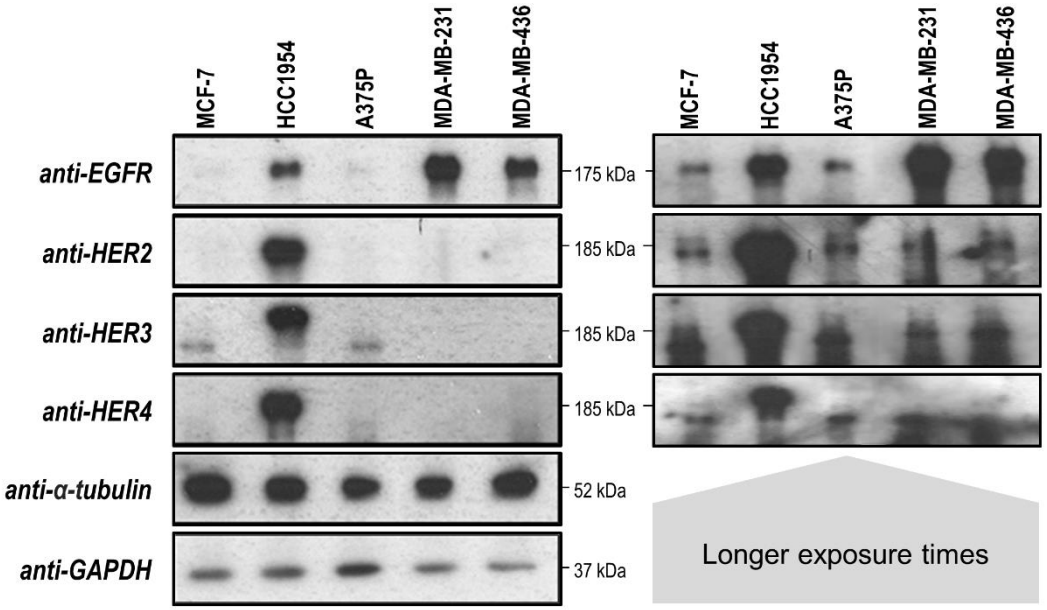

Supplementary Figure S5. Immunoblot analysis of ErbB family proteins in breast cancer cell lines used in this study | Cell lysates from indicated cell lines were normalised for protein content (BCS assay) and subjected to SDS-PAGE followed by protein transfer to PVDF membranes and detection of indicated proteins. The breast cancer cell lines MDA-MB-231, MDA-MB-436 (both triple-negative) and HCC1954 and MCF-7 all express ErbB family members, in line with literature data.

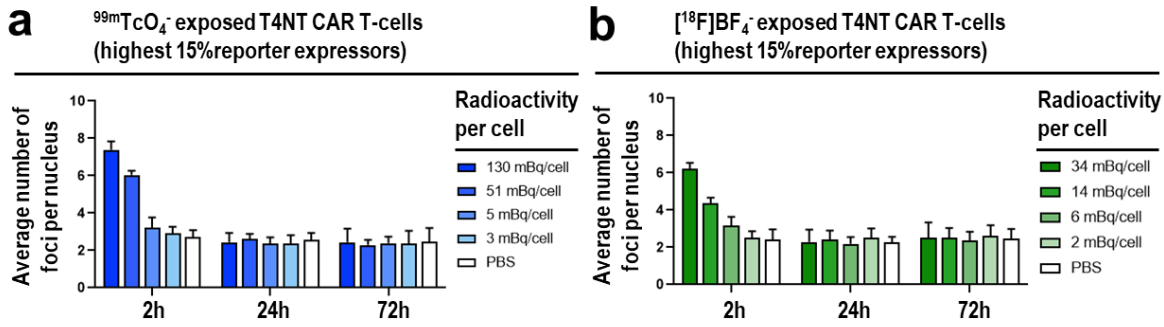

Supplementary Figure S6. Additional data to Fig.3D. | Data shown are representative of the highest 15% of the CAR-reporter platform expressors. This subset of data from Fig.3D/left demonstrated dose-dependency of NIS expression and indicated more detected foci in highest NIS expressors, consistent with higher radiotracer uptake. Error bars are SD; *N*=3 experiments with a total of >35 cells each analysed.

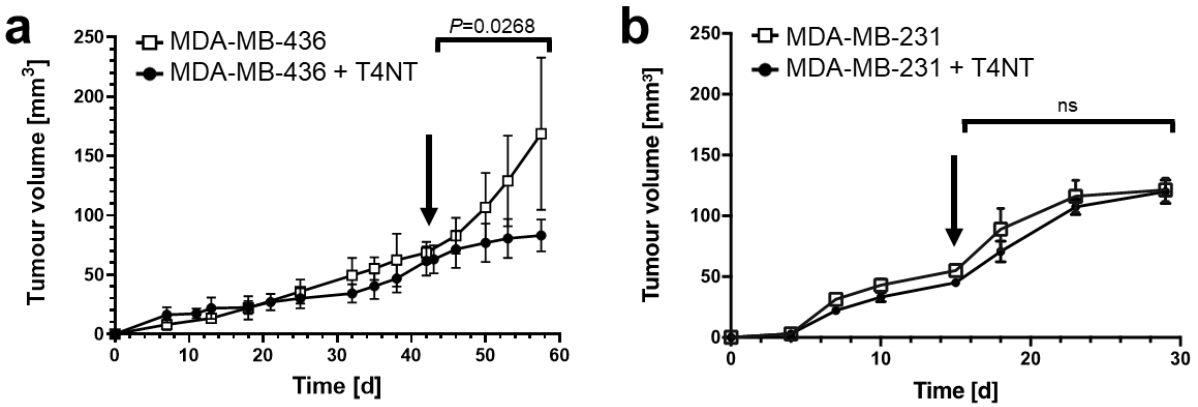

Supplementary Figure S7. Tumour growth curves for *in vivo* experiments shown in Fig.5 and Fig.6 | (A) Cumulative tumour growth curves for MDA-MB-436 xenograft models in NSG mice. **(B)** Cumulative tumour growth curves for MDA-MB-231 xenograft models in NSG mice. Tumour volumes did not significantly differ between cohorts of individual tumour models at the time of immunotherapy administration (arrows). After immunotherapy administration, tumour growth was significantly reduced over time in the MDA-MB-436 model but not in the MDA-MB-231 model (Pearson correlation analysis; two-tailed; including measurements at the day of administration). Error bars represent SD.

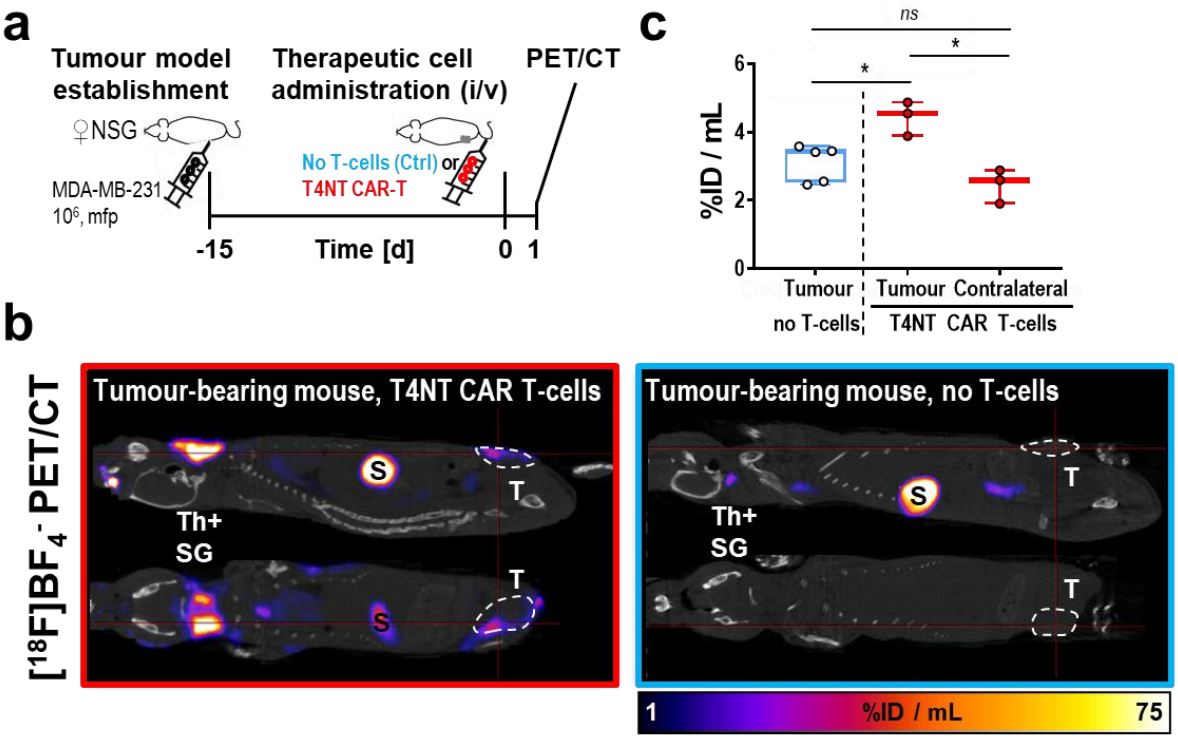

Supplementary Figure S8. Intravenously administered T4NT CAR T-cells home to the primary tumour in MDA-MB-231 tumours | (A) Experimental scheme. **(B)** Either $5x10^6$ T4NT CAR T-cells (red frame) or vehicle (blue frame) were intravenously administered on day zero and animals were PET/CT imaged (5 MBq $[^{18}F]BF_4^-$; 40 min post administration) 24h later. Endogenous signals are recorded in the thyroid and salivary glands (Th+SG), the stomach (S) and at much lower levels in some regions of the mammary glands. Tracer excretion happened renally, which is why in some animals, depending on their bladder fill status before imaging, signals from the bladder were recorded (B). T4NT CAR T-cells were detected in the tumour area but their distribution was not uniform within the tumours. Anatomical imagines (CT; grayscale) are overlayed with PET images (hue). Coronal and sagittal slices from a representative animal per cohort are shown; all PET images are on the same scale. **(C)** Cumulative quantitative analysis of whole-tumour radioactivity from *in vivo* images ($N \geq 3$). Box shows range from 25th to 75th percentile, whiskers minimum and maximum values; each dot represents one mouse; * indicates $P<0.05$.

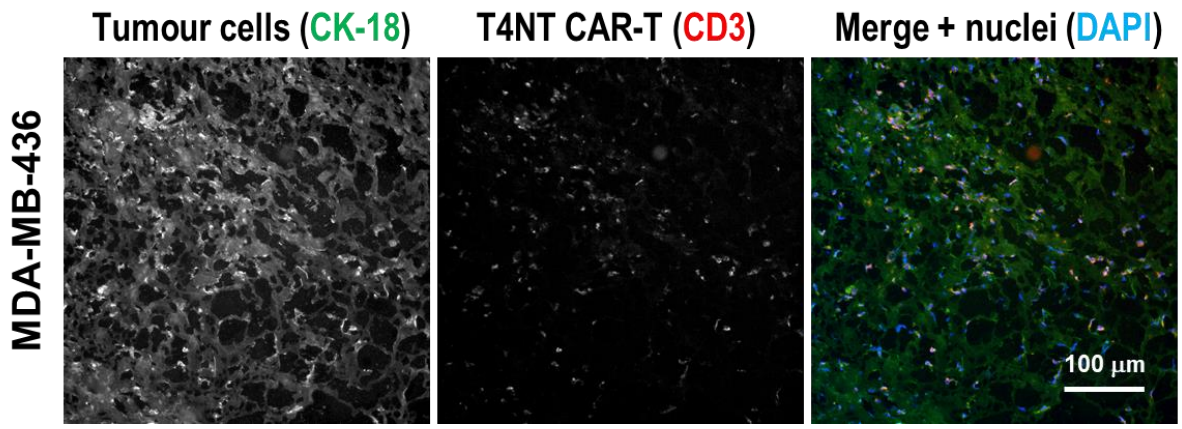

Supplementary Figure S9. Histology of MDA-MB-436 tumour treated with T4NT CAR T-cells | Immunofluorescence histology demonstrating T4NT CAR T-cell presence within the tumour mass of MDA-MB-436 tumours that received T4NT (*cf.* experiment in Fig.6). Tumour cells were visualized by staining with anti-human cytokeratin-18 and T4NT with anti-human CD3. Representative micrographs are shown. Scale bars is 100 µm.

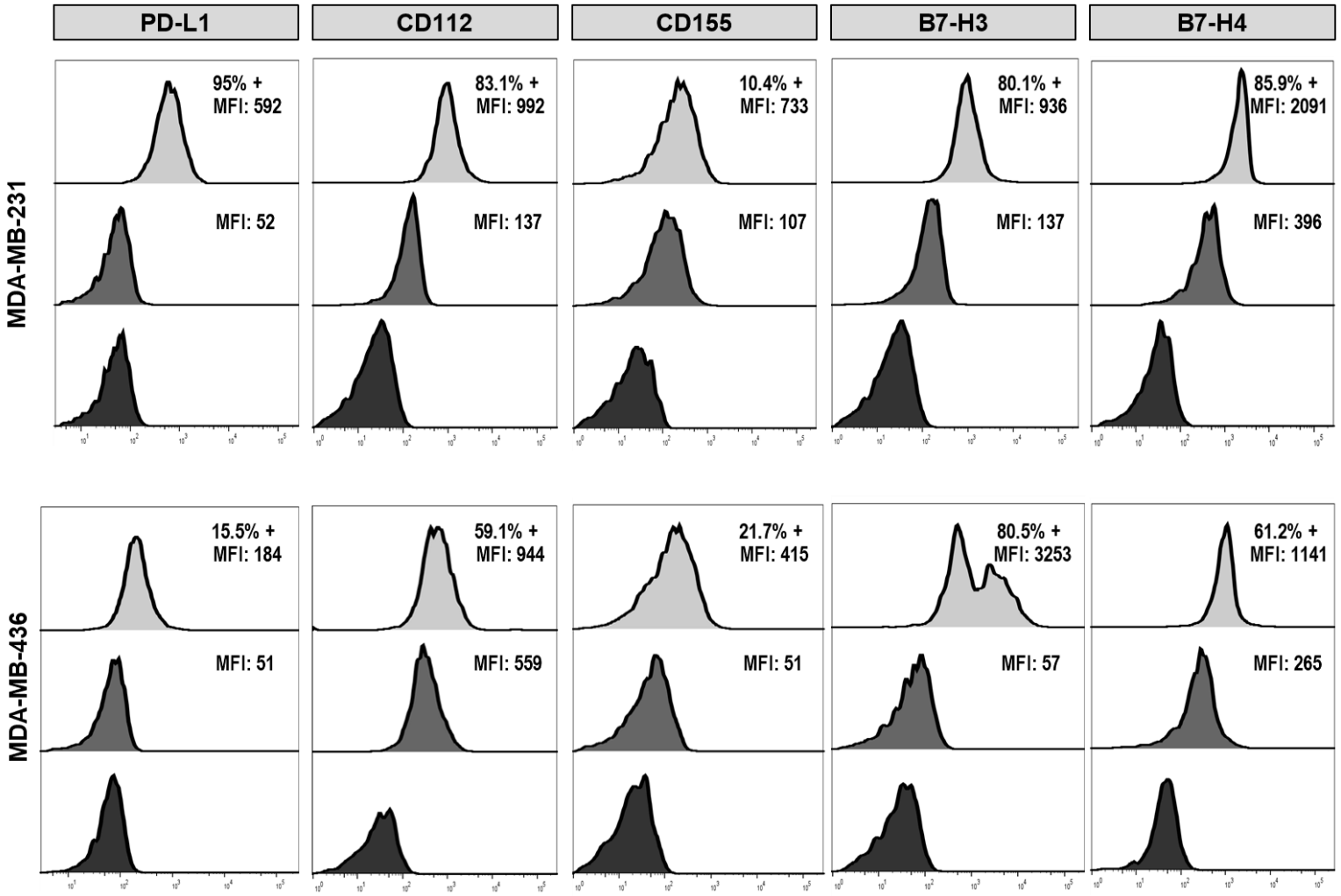

Supplementary Figure S10. Representative flow cytometry histograms complementing data in Fig.8 | Stacked flow cytometry histograms of stained samples, FMO controls and unstained cell samples for the indicated antibodies. One representative determination is shown. Cumulative data are shown in Fig.8.

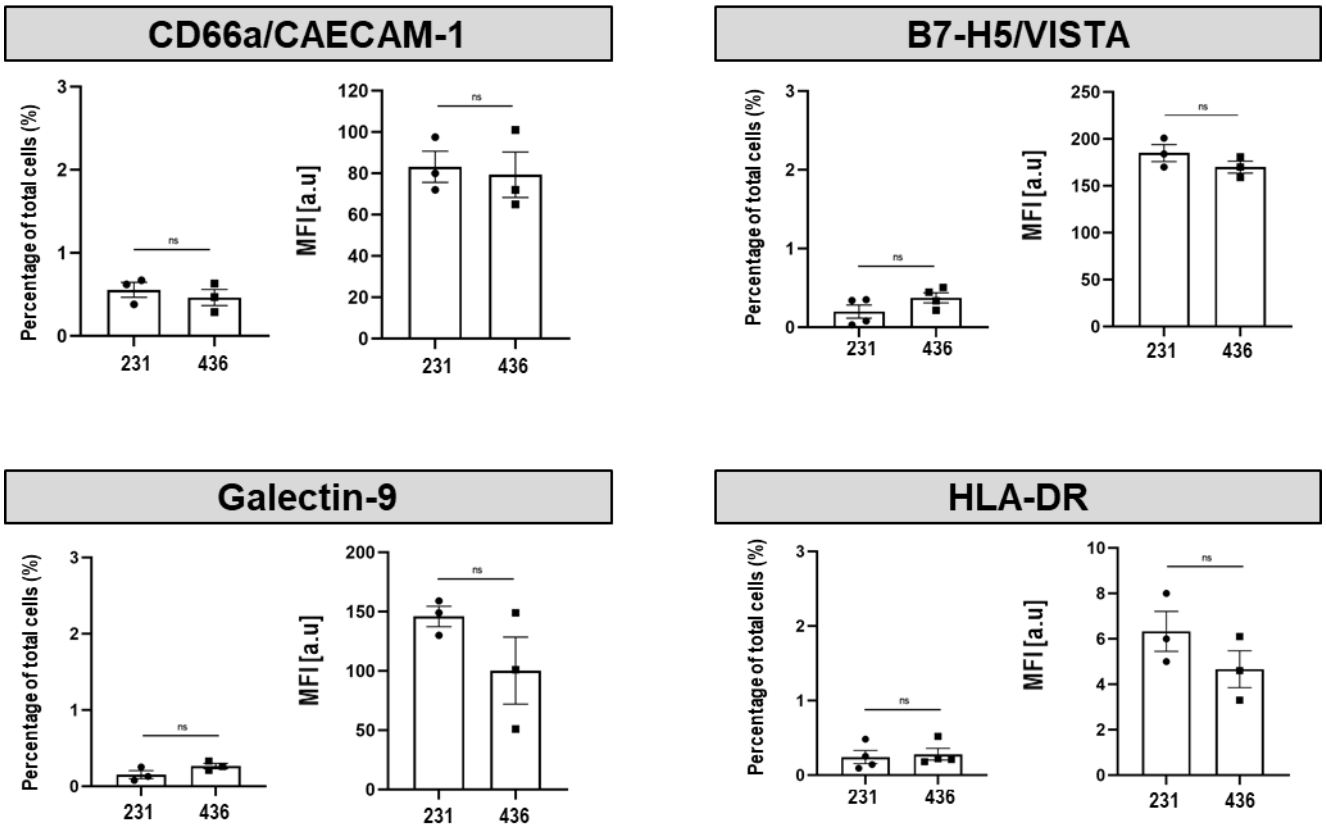

Supplementary Figure S11. Additional BCC analyses complementing data in Fig.8. | BCC lines were stained with antibodies directed against the indicated cell-surface proteins known to constitute one part of an immune checkpoint axis or a B7-class inhibitory molecule. Analysis was by flow cytometry using (left) FMO controls to categorize cells into populations positive or negative for the indicated molecule, while (right) obtained MFI values were compared between cell lines. Error bars represent SD; *N*=3 independent determinations.

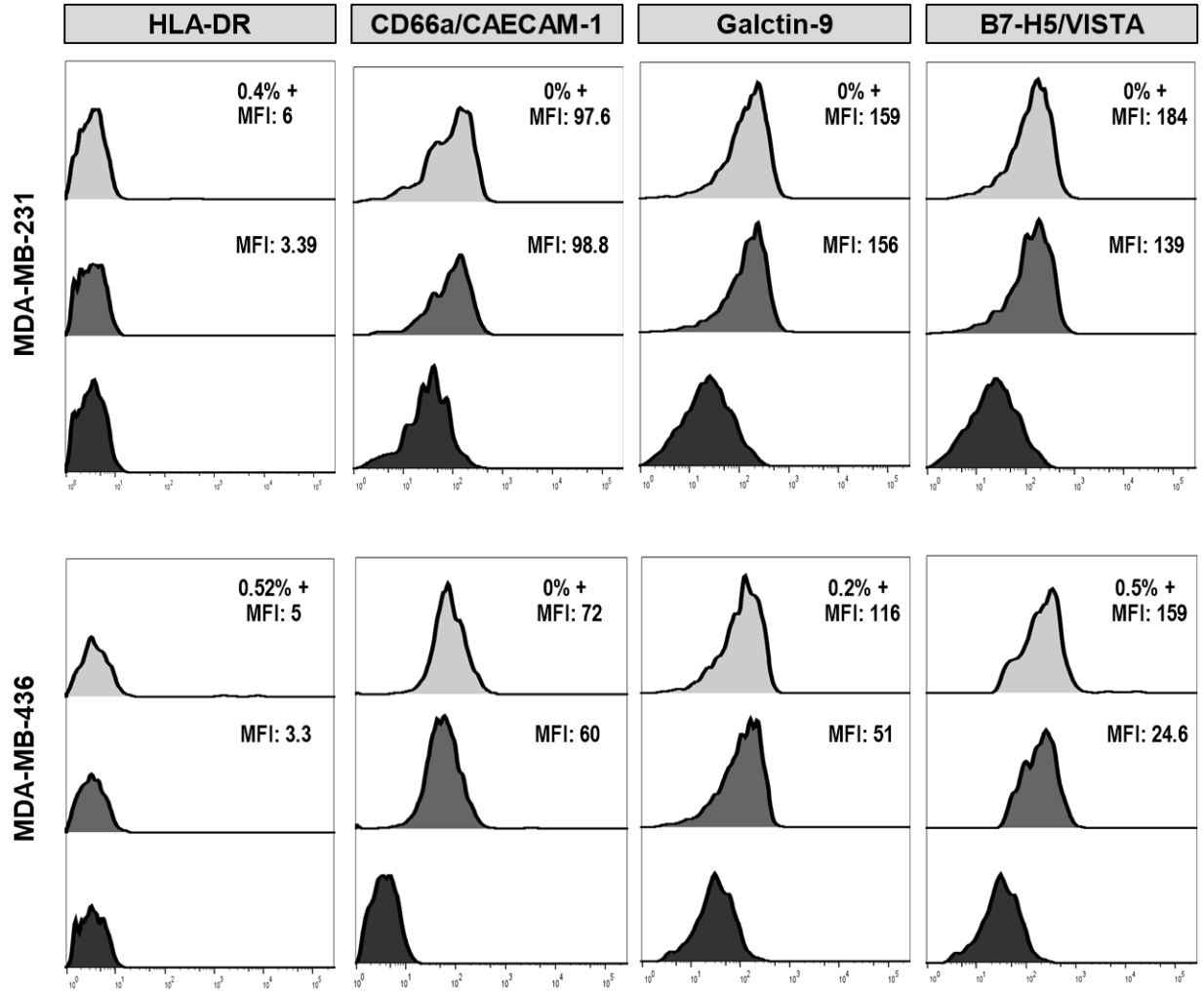

Supplementary Figure S12. Representative flow cytometry histograms complementing data in Supplementary Fig.S11 | Stacked flow cytometry histograms of stained samples, FMO controls and unstained cell samples for the indicated antibodies. One representative determination is shown. Cumulative data are shown in Fig.S11.

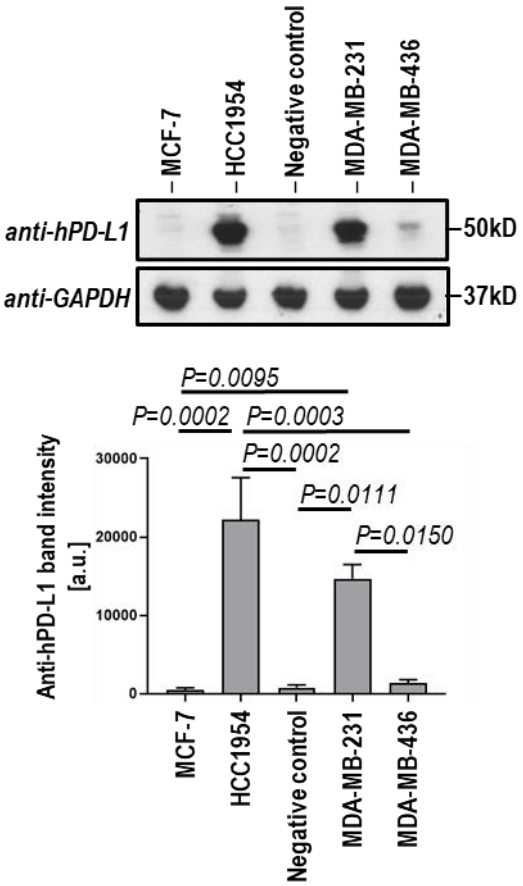

Supplementary Figure S13. Immunoblot analysis of different breast cancer cell lines for PD-L1 | Indicated TNBC lines MDA-MB-436 and MDA-MB-231, a negative control (rat adenocarcinoma cell line), MCF-7 and HCC10954 cell lines were subjected to immunoblot analysis (to also provide context of relative PD-L1 expression by a method independent to flow cytometry). (*Top*) Representative immunoblot. (*Bottom*) Cumulative immunoblot analysis; error bars are SD; *N*=3; *P*-values by ANOVA with Tukey's multiple comparison test.

***** End of Supplementary Information *****